Article

Immunity

# Network Integration of Parallel Metabolic and Transcriptional Data Reveals Metabolic Modules that Regulate Macrophage Polarization

## Highlights

- Glutamine deprivation affects M2 polarization but not M1 polarization
- UDP-GlcNAc biosynthesis and N-glycosylation are important for M2 polarization
- There is no reverse or direct flow through Idh or malic enzyme in M1 macrophages
- Aspartate-arginosuccinate shunt connects the NO and TCA cycles in M1 polarization

## Authors

Abhishek K. Jha,
Stanley Ching-Cheng Huang, ...,
Edward M. Driggers,
Maxim N. Artyomov

## Correspondence

edward.driggers@generalmetabolics.com (E.M.D.),
martyomov@pathology.wustl.edu (M.N.A.)

## In Brief

Polarization of macrophages involves a metabolic and transcriptional rewiring that is only partially understood. Artyomov and colleagues used an integrated high-throughput transcriptional-metabolic profiling and analysis pipeline to identify metabolic modules that support macrophage polarization and function.

## Accession Numbers

GSE53053

Jha et al., 2015, Immunity *42*, 419–430
March 17, 2015 ©2015 Elsevier Inc.
http://dx.doi.org/10.1016/j.immuni.2015.02.005

CellPress

# Network Integration of Parallel Metabolic and Transcriptional Data Reveals Metabolic Modules that Regulate Macrophage Polarization

Abhishek K. Jha,[1] Stanley Ching-Cheng Huang,[2] Alexey Sergushichev,[2,3] Vicky Lampropoulou,[2] Yulia Ivanova,[2] Ekaterina Loginicheva,[2] Karina Chmielewski,[1] Kelly M. Stewart,[1] Juliet Ashall,[2] Bart Everts,[2,5] Edward J. Pearce,[2,4] Edward M. Driggers,[1,4,6,*] and Maxim N. Artyomov[2,4,*]
[1]Agios Pharmaceuticals, 38 Sidney Street, Cambridge, MA 02139, USA
[2]Department of Pathology & Immunology, Washington University in St. Louis, 660 S. Euclid Avenue, St. Louis, MO 63110, USA
[3]ITMO University, 49 Kronverksky Prospekt, Saint Petersburg 197101, Russia
[4]Co-senior author
[5]Present address: Department of Parasitology, Leiden University Medical Center, Albinusdreef 2, Leiden 2333 ZA, the Netherlands
[6]Present address: General Metabolics, 30 Arlington Street, Winchester, MA 01890, USA
*Correspondence: edward.driggers@generalmetabolics.com (E.M.D.), martyomov@pathology.wustl.edu (M.N.A.)
http://dx.doi.org/10.1016/j.immuni.2015.02.005

## SUMMARY

**Macrophage polarization involves a coordinated metabolic and transcriptional rewiring that is only partially understood. By using an integrated high-throughput transcriptional-metabolic profiling and analysis pipeline, we characterized systemic changes during murine macrophage M1 and M2 polarization. M2 polarization was found to activate glutamine catabolism and UDP-GlcNAc-associated modules. Correspondingly, glutamine deprivation or inhibition of N-glycosylation decreased M2 polarization and production of chemokine CCL22. In M1 macrophages, we identified a metabolic break at *Idh*, the enzyme that converts isocitrate to alpha-ketoglutarate, providing mechanistic explanation for TCA cycle fragmentation. $^{13}$C-tracer studies suggested the presence of an active variant of the aspartate-arginosuccinate shunt that compensated for this break. Consistently, inhibition of aspartate-aminotransferase, a key enzyme of the shunt, inhibited nitric oxide and interleukin-6 production in M1 macrophages, while promoting mitochondrial respiration. This systems approach provides a highly integrated picture of the physiological modules supporting macrophage polarization, identifying potential pharmacologic control points for both macrophage phenotypes.**

## INTRODUCTION

The ability to assume different activation states in response to environmental factors is critical to the role played by murine macrophages in a broad range of responses. Resting macrophages (M0) develop pro-inflammatory microbicidal and tumoricidal properties after stimulation with interferon-γ (IFN-γ) and toll-like receptor (TLR) agonists (M1 or classical activation), but they will promote adipose tissue homeostasis and wound healing and mediate anti-helminth immune responses when stimulated with interleukin-4 (IL-4) and IL-13 (M2 or alternative activation). This phenotypic polarization of murine macrophages in response to their microenvironment is highly regulated at both transcriptional and metabolic levels (McGettrick and O'Neill, 2013; O'Neill and Hardie, 2013).

The metabolism of M1 macrophages is characterized by increased glycolytic flux and reduced mitochondrial oxidative phosphorylation compared to M0 cells (Rodríguez-Prados et al., 2010). This metabolic shift occurs in the context of an altered TCA cycle, which is needed to support the production of key M1 cellular products such as acetyl CoA (AcCoA), succinate, and nitric oxide (NO) (Tannahill et al., 2013). However, the precise metabolic flows that alter the mitochondrial activity and the corresponding compensatory mechanisms that maintain basic cellular metabolic functions in the absence of an active TCA cycling in M1 macrophages are unclear. Likewise, although it is understood that M2 activation is coupled to changes in polyamine synthesis, iron metabolism, and fatty acid oxidation (Biswas and Mantovani, 2012; Vats et al., 2006), we currently lack a systems-level understanding of central metabolic rewiring during alternative activation.

In principle, integration of top-down transcriptional and metabolic "omics" approaches provide a strategy for non-targeted characterization of systems-level changes, but two obstacles impede realization of such a strategy. First is the lack of parallel experimental approaches to enable synchronized metabolomic and transcriptional profiling on simultaneously prepared biomass; the throughput of current experimental approaches for metabolic profiling are typically quite low and require a considerable amount of input material, making it difficult to perform parallel sample preparation for transcriptional profiling. A second challenge is the uncertainty associated with integrating the two data types in a physiologically meaningful way that can be further validated through functional testing. Here, we introduce a combined experimental and computational pipeline, concordant metabolomics integration with transcription (CoMBI-T),

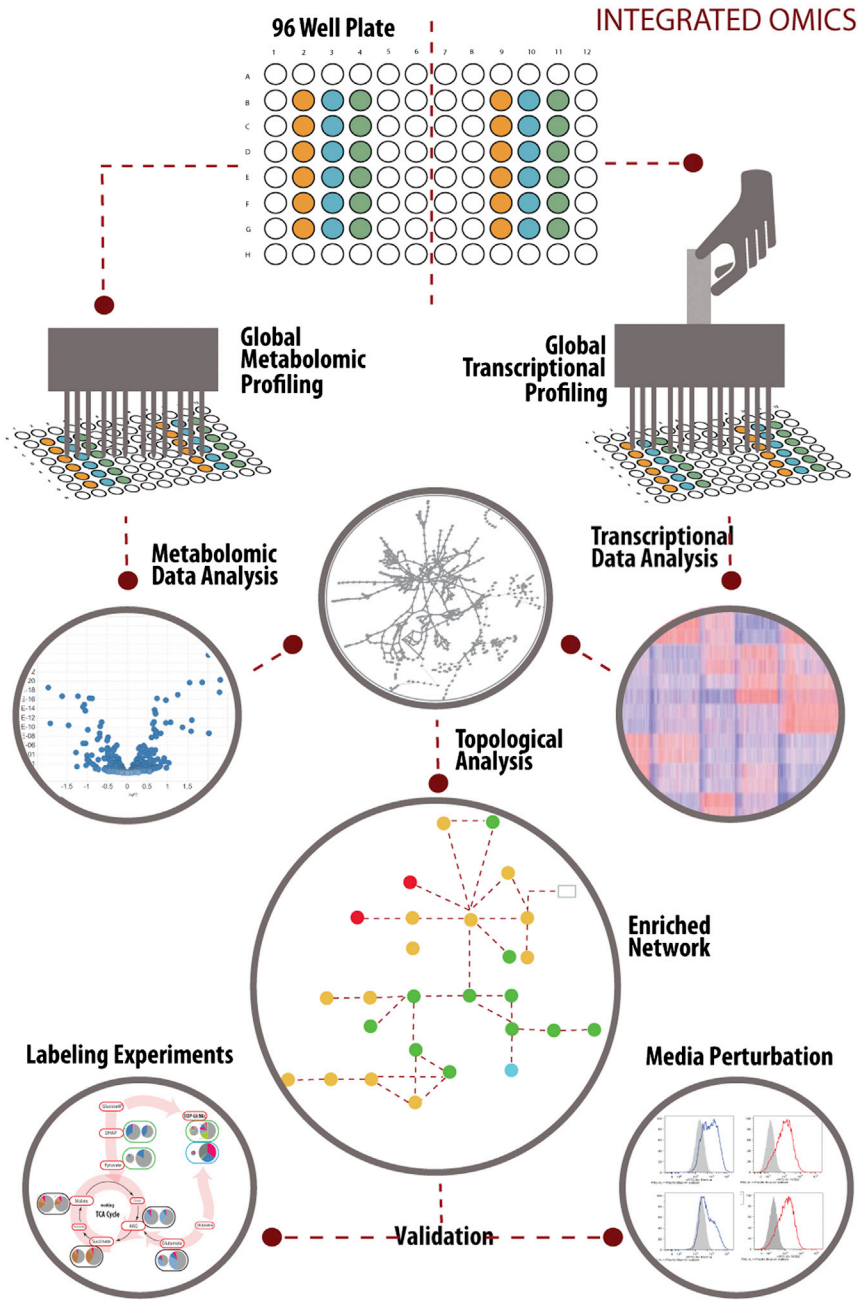


**Figure 1. Integrated Metabolic-Transcriptional Profiling and Analysis Pipeline**

Cells derived from the same culture batch are grown in 96-well plates, stimulated, then lysed and processed in 96-well format to collect global metabolic and RNA-seq-based transcriptional profiles. Individual datasets are then processed and differential regulation data are mapped onto a global metabolic network that includes both enzymes and metabolites. Integrated network analysis then identifies the most coordinately responsive subnetwork and uncovers novel points of metabolic rewiring during macrophage polarization. Predictions of CoMBI-T profiling analysis are then validated mechanistically through labeling experiments and through the effects of targeted media perturbation and pharmacologic agents on cell phenotype.

that overcomes these challenges and provides a non-targeted systems-level characterization of coordinated transcriptional and metabolic rewiring during the macrophage polarization process. This approach identified statistically significant modules within the metabo-transcriptional network that contribute to and define M1 versus M2 polarization, which were functionally validated via a combination of targeted media perturbations, pharmacological inhibition, and $^{13}$C-glucose and $^{13}$C- and $^{15}$N-glutamine labeling experiments. In M2-polarized macrophages, CoMBI-T reveals involvement of two new previously uncharacterized modules: a glutamine-associated module and a UDP-GlcNAc-associated module. Perturbation of either of these pathways led to impairment of M2 polarization. Furthermore, glutamine deprivation is shown to be associated with profound functional consequences in M2 macrophages, such as decreased chemokine *Ccl22* production. On the other hand, in M1 macrophages, CoMBI-T identified a metabolic interruption in the tricarboxylic acid (TCA) cycle carbon flow during M1 polarization, which was validated by isotope labeling. Based on that labeling data, we propose that a variant of the aspartate-arginosuccinate shunt connects the fragmented (anapleurotic) TCA cycle metabolites with NO production during the inflammatory response. Consistent with this model, inhibition of a key enzyme in the shunt, aspartate aminotransferase (AAT), led to decreased NO production and increased oxygen consumption rates (OCR) due to mitochondrial respiration in M1 macrophages. Overall, our data and analysis provide a comprehensive view of the integrated transcriptional and central metabolic changes during murine macrophage polarization, yielding a deeper contextual understanding of established polarization markers, while simultaneously uncovering targets for pharmacological intervention and control of the polarization process.

## RESULTS

### CoMBI-T Data Acquisition: Parallel High-Throughput Metabolic and Transcriptional Profiling

The CoMBI-T pipeline to generate and integrate mass spectrometry-based metabolic profiling with RNA-seq-based transcriptional profiling data sets is shown schematically in Figure 1. To provide the raw biological material for the data acquisition, bone marrow cells were isolated from a single mouse and seeded into 96-well plates as described previously (Everts

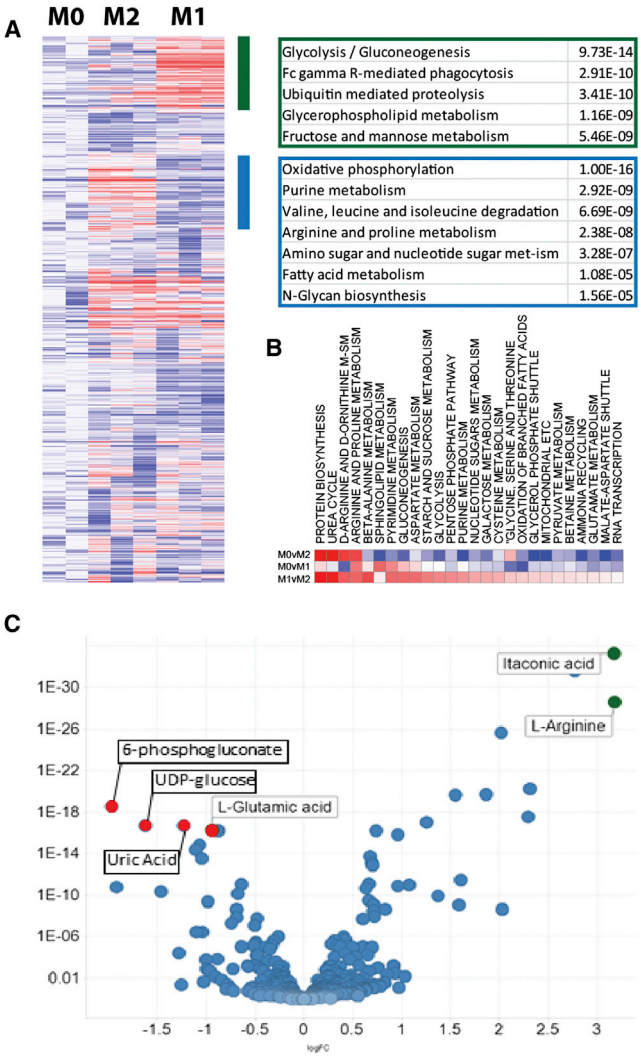


**Figure 2. Knowledge-Based Pathway Analysis of Metabolic and Transcriptional Data**

(A) Pathway analysis of enzymes that are transcriptionally upregulated in M1 or M2 states. Green bar points to the enzymes upregulated in M1 conditions (blue for M2) and corresponding enriched pathways are listed in the green box on the right (blue for M2).

(B) Pathway enrichment analysis across metabolome profiling data shows KEGG pathways that are differentially regulated between all possible pairs of conditions (M1 versus M0, M2 versus M0, M1 versus M2).

(C) Volcano plot shows metabolites differentially expressed between M1 and M2 conditions. *x* axis shows log-fold change between M1 and M2 conditions with positive values corresponding to metabolites upregulated in M1 macrophages. *y* axis shows p value for corresponding metabolite. Top M1-specific metabolites (itaconate and arginine) are highlighted in green, and top M2-specific metabolites are marked as red circles.

et al., 2014). At day 7, the bone-marrow-derived macrophages (BMDMs) were stimulated with either lipopolysaccharide (LPS) and IFN-γ or IL-4 treatment for 24 hr to obtain M1- and M2-polarized cells (respectively, as confirmed by expression of major markers such as *Il12b*, *Nos2*, *Arg1*, etc.). Cultures destined for either of the two analyses were treated identically until cells were lysed for metabolite and RNA extractions, providing minimal divergence in cell handling and maximum degree of consistency between metabolic and transcriptional profiles. To obtain metabolic profiles, we used a non-targeted, flow-injection-analysis (FIA) mass spectrometry (MS) method (Fuhrer et al., 2011), enabling broad metabolite coverage between 50 and 1,000 daltons and yielding quantitative information on approximately 10,000 MS spectral features (Fuhrer et al., 2011), of which approximately 2,200 were annotated as high-confidence metabolites in these studies. For transcriptional profiling, we used 3′ end focused RNA sequencing with a barcode-first strategy that allows sample pooling at the cDNA stage, improving sensitivity and consistency between samples and allowing construction of a high-throughput library from material extracted from cell lysates in a single well of a 96-well plate (Sojka et al., 2014) (Experimental Procedures). Overall, we analyzed five and three bio-replicates per condition for metabolic and transcriptional profiles, respectively.

## CoMBI-T Analysis: Network-Based Integration of High-Throughput Metabolic and Transcriptional Profiles

To date, predictive powers of integrated analysis have been tested only to a very limited degree, largely due to a lack of large-scale, parallel metabo-transcriptional datasets. Overall, analytical strategies used for integration of metabolic and transcriptional data can be broadly divided into two major classes: modifications of constraint-based models (such as flux balance analysis) (Bordbar et al., 2012; Patil and Nielsen, 2005) and network-based approaches (Beisser et al., 2012; Zhu et al., 2012). In order to leverage the large metabolite coverage achieved in our profiling experiments, we adopted a network-based strategy that integrates the power of both transcriptional and metabolic profiles while minimizing the drawbacks inherent to each dataset with respect to computational analysis. For instance, metabolic profiling often has a high false negative rate, being neither exhaustive nor adequately sensitive for low-abundance metabolites. Nevertheless, metabolism is described by a relatively well-defined network, capturing the interconversion of various metabolites in a framework particularly suitable for systems-scale analysis. The opposite is true for transcriptional data: RNA-seq profiling provides an exhaustive list of mature transcripts, but their corresponding regulatory networks are defined very loosely, limiting the ability to follow causal relationships. Our integration strategy seeks to identify functional modules characteristic to the M1 and M2 states based on proximity of differentially regulated metabolites and enzymes in the global metabolic network. Such core subnetworks typically consist of combinations of metabolites and enzymes from multiple canonical metabolic pathways (see examples below) and provide relatively unbiased characterization of metabolic changes in the system of interest.

As such, this approach differs from the typical knowledge-based pathway enrichment analysis (PEA) because it allows the capture of major routes of metabolic rewiring that occur on a global level but that do not necessarily follow known definitions of pathways. For instance, pathway analysis of obtained metabolic and transcriptional profiles (Figure 2A) revealed a combination of known pathways regulating macrophage polarization without specific understanding of functional interconnections between them. Genes involved in glycolysis and phospholipid

metabolism, differentially expressed between M1 (LPS + IFN-γ stimulation) and M2 (IL-4 stimulation) macrophages, are major distinguishing features of inflammatory (M1) macrophages, whereas oxidative phosphorylation, purine synthesis, arginine, and nucleotide sugar metabolism are enhanced in M2 macrophages. Global metabolic changes showed differential regulation of glycolysis/gluconeogenesis, urea cycle, arginine, mitochondrial, and fatty acid metabolism (Figure 2B). However, the interpretative utility of these findings is severely limited because the interconnections between these pathways are not revealed even though macrophage polarization requires them to be globally coordinated. Furthermore, pathway-based analysis fails to account for many of the most differentially expressed metabolites: in M1 macrophages itaconic acid (Figure 2C, green circle) is currently not annotated to be the part of any individual pathway, and a number of the most altered M2 metabolites such as UDP-glucose and 6-phosphogluconate (Figure 2C, red circles) are not associated with any of the enriched pathways. Finally, pathway analyses that are carried out on the individual levels of regulation (whether transcriptional or metabolic) inherently fail to leverage the notion of coherent changes between these regulatory events, diminishing their power to identify important regulators of metabolic rewiring.

In order to address these issues, we constructed a global murine cellular reaction network (CRN) that connects ~3,000 metabolites and corresponding enzymes based on the latest edition of the KEGG database (Kanehisa et al., 2012) (see Experimental Procedures). We then sought the most differentially regulated subnetwork (typically of the size ~100 nodes) within the CRN, accounting for both the nodal connectivity and the degree of differential expression of metabolites and enzymes in the network. We first assign weights to nodes in the global cellular reaction network: differential expression p values for M1 versus M2 comparison were transformed to enzymatic node weights, and differential intensity p values of metabolites corresponded to metabolic node weights. By structuring the CRN in this manner, we were able to apply the BioNet algorithm (Beisser et al., 2010), developed for integration of protein-protein interaction databases with microarray datasets, to identify the most differentially regulated network as a maximum-weight connected subgraph (MWCS) problem (Figure 3; Experimental Procedures). Overall, CoMBI-T analysis indicated that divergent macrophage polarization is characterized by significant differences in three metabo-transcriptional modules (the UDP-GlcNAc biosynthesis module, a glutamine/glutamate-associated module in M2 macrophages, and an *Idh*-centered TCA pathway break-point coupled with dramatic itaconate production in M1-polarized macrophages) that together with known regulatory pathways make up a densely connected core that governs macrophage metabolic response to polarization stimuli (Figure 3). Next, we sought to investigate the function of these modules in greater detail.

## CoMBI-T Reveals Increased UDP-GlcNAc Synthesis as a Critical Feature of M2 Polarization

CoMBI-T identified two previously unreported M2-specific metabolic modules. First, increased amino sugar and nucleotide sugar metabolism, characterized by high levels of UDP-GlcNAc, UDP-glucose, and UDP-glucuronate, and corresponding transcriptional upregulation of enzymes involved in the production of these intermediates (e.g., Enpp1, Pgm1), were observed in M2 macrophages (Figure 3). To validate that this module is indeed metabolically active in M2-polarized macrophages, we traced the fate of $^{13}$C-glucose and $^{13}$C-glutamine in M2 cells to the intermediates of these pathways. Labeling distribution analyses revealed partially labeled forms of TCA metabolites (malate, citrate, AKG, succinate) in M0 and M2 macrophages (Figure 4A), reflecting reported active oxygen consumption rates and complete TCA cycling in M2 macrophages (Haschemi et al., 2012). Consistent with the known hexosamine biosynthetic route, we found glucose and glutamine as the major sources of carbon and nitrogen, respectively, in UDP-GlcNAc, an important intermediate that links signaling to metabolism (Figure 4A; Wellen and Thompson, 2012; Yi et al., 2012). Together with transcriptional upregulation of steps in the N-glycan pathway revealed through pathway enrichment analysis (see Figure 2A), this observation suggests the importance of N-glycosylation in M2 macrophages. It is well established that highly glycosylated lectin/mannose receptors are among the most typical M2 polarization markers (Sica and Mantovani, 2012). We investigated the functional importance of the UDP-GlcNAc pathway by asking directly whether N-glycosylation plays a role in M2 activation. Accordingly, we stimulated macrophages with IL-4 in the presence or absence of the N-glycosylation inhibitor tunicamycin (Varki, 2009). We found that tunicamycin significantly inhibited expression of the canonical M2 activation markers Relmα (Figure 4B), CD206, and CD301 (Figure 4C), only mildly affecting M1 polarization as measured by inducible nitric oxide synthase (iNOS) protein expression (Figure S1A) or regulation of major M1-specific cytokines (Figure S1B). Similarly, M2-specific defects were observed when we inhibited the hexosamine pathway via glucosamine (Figure S1C; Koch et al., 1979). Thus, the UDP-GlcNAc synthesis pathway identified by CoMBI-T as being upregulated in M2 macrophages plays a direct, specific, and critical role in the M2 polarization process.

## CoMBI-T Reveals Glutamine Metabolism as a Characteristic Feature of M2 Polarization

The second M2-specific module revealed by CoMBI-T was centered on glutamate management and included glutamate, AKG, ornithine, and corresponding transcripts of *Gatm*, *Arg1*, *Oat*, *Got2*, and *Gpt2* as well as several other closely related transcripts and metabolites (Figure 3). This result together with the participation of glutamine in supporting an active TCA cycle and providing structural features for UDP-GlcNAc synthesis led us to hypothesize that this amino acid plays a crucial, specific role in M2 polarization. The extent of glutamine dependence in M2 macrophages was suggested by the fact that a third of all carbons in TCA metabolites in M2 cells originated from glutamine (versus ~20% for M1) and that within 4 hr of addition of $^{15}$N-labeled glutamine, more than half of the nitrogen in UDP-GlcNAc derived from glutamine (Figure 4A). To functionally validate these findings from CoMBI-T, we transiently (for 4 hr prior to stimulation) deprived macrophages of glutamine and assessed M2 commitment, using expression of CD206, CD301, and Relmα as markers of M2 activation. We found that glutamine deprivation had a substantial effect on M2 polarization, reducing the committed population by

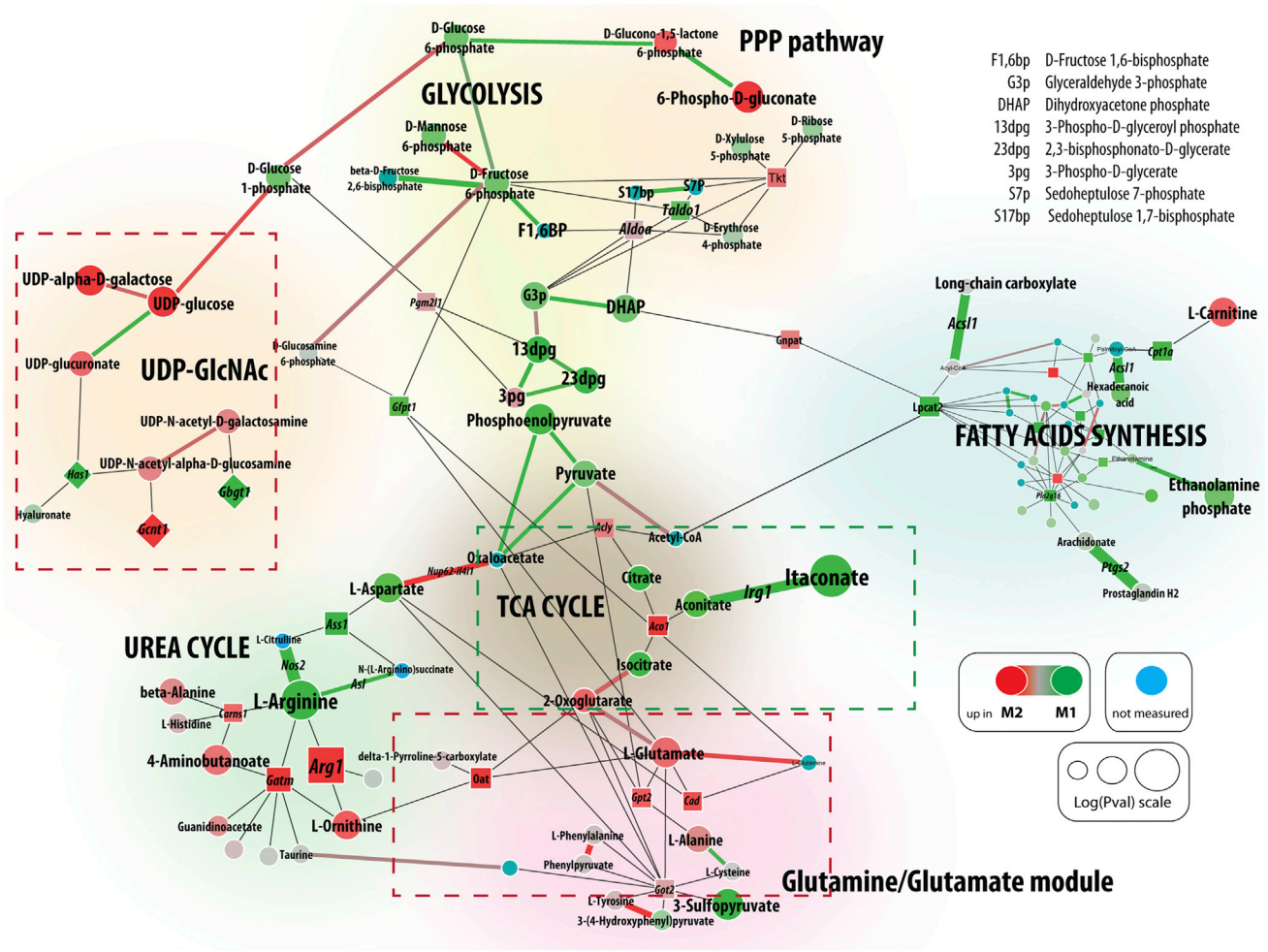


**Figure 3. Major Metabolic Modules Are Rewired during Macrophage Polarization**

CoMBI-T reveals the most regulated subnetwork within global murine metabolic network that consists of more than 2,000 enzymes and metabolites measured through the CoMBI-T profiling pipeline. For comparison between M1- and M2-polarized macrophages, the most regulated metabolic subnetwork encompasses seven distinct modules highlighted by distinct background shading. Three major novel features of macrophage polarization identified by CoMBI-T are highlighted with dotted line squares—green for M1-specific module and red for M2. Round nodes represent metabolites within core regulatory network. Enzymes are represented by square nodes. Differential expression of corresponding enzyme/metabolite is indicated by the size of the node, and fold-change by red (M2) to green (M1) color scale. Enzymes in reactions with single product-substrate pair are represented by edges for visual convenience with thickness and color of the edge reflecting –log(p) and fold-change of differential expression correspondingly. For visual convenience, nodes of fatty acid synthesis module are not labeled. The complete metabolomic data used for CoMBI-T are available in Table S1.

about 50% (Figure 5A), whereas removal of glutamine had no effect on capacity for M1 polarization as measured by Nos2 upregulation (Figure 5B).

We next sought to determine specific functional defects in M2-polarized macrophages due to glutamine deprivation. We obtained transcriptional profiles for macrophages polarized in either complete media or in glutamine-deprived media and found that most of the differentially expressed transcripts that are downregulated upon glutamine withdrawal are M2-specific marker genes, including *Irf4*, *Klf4*, *Ccl22*, and *Il4i1*. Notably, glutamine-deprived M2 macrophages exhibited a distinctly downregulated transcriptional signature of TCA cycle activity (Figure 5C) when compared to M2 macrophages polarized in full media, thus providing support for a causal link between glutamine usage, regulation of oxidative phosphorylation, and M2 polarization, as opposed to other possibilities such as an effect via the mTOR pathway (Byles et al., 2013), which was not regulated upon glutamine deprivation (Figures S2A–S2C). This is consistent with literature reporting that transient glutamine deprivation in a human cell line led to perturbation of TCA cycle and autophagy as opposed to the activation of mTOR signaling typically seen in more severe starvation conditions (Shanware et al., 2014). Strikingly, the chemokine pathway (Figure S2B) was found to be among those most downregulated upon glutamine deprivation, and therefore we tested the effect of glutamine depletion on production of CCL22, because expression of the encoding gene *Ccl22* is markedly upregulated in M2 macrophages and it is the second most-downregulated transcript upon glutamine deprivation ($p = 10^{-57}$; Figure 5D, in red are shown transcripts that are

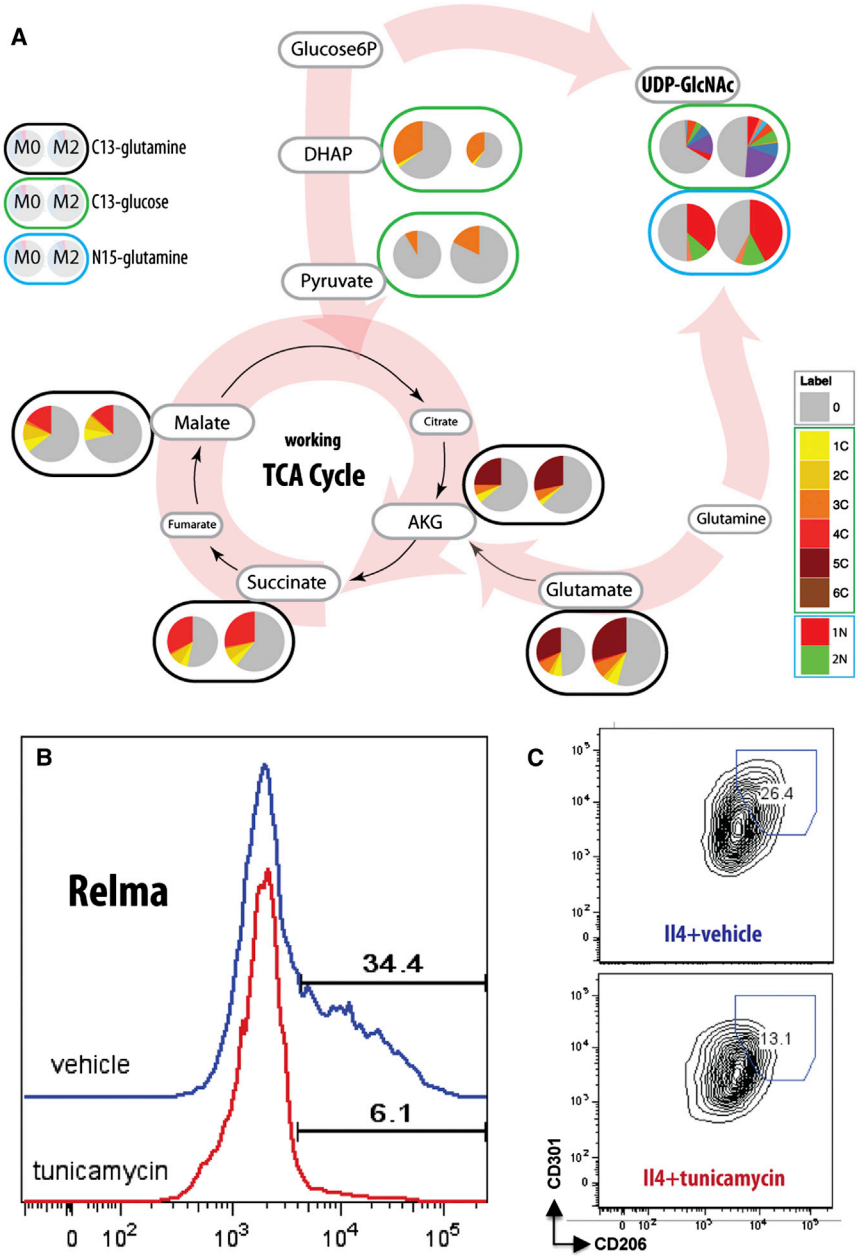


**Figure 4. Labeling and Pharmacological Inhibition Experiments Validate the Critical Role of UDP-GlcNAc Pathway in M2 Polarization**

(A) U-$^{13}$C glucose (green outline) and U-$^{13}$C (black outline), $^{15}N_2$ (blue outline) glutamine were used as media for unstimulated/Il4-stimulated macrophages. Circle sizes are scaled with respect to pool sizes for individual metabolites in each condition. Exact labeling distributions and patterns are detailed in Table S2 for each metabolite. Thin black arrows represent known metabolic pathway connections; background arrows indicate deduced major metabolic flows in M2 macrophages.

(B and C) Results of inhibition of N-glycosylation by tunicamycin: in the presence of the inhibitor, M2 commitment is significantly blocked by both Relmα (B) and CD206-CD301 staining (C).

M2-specific up- or downregulated markers). Accordingly, secreted protein levels of CCL22 was lower in supernatants of M2 macrophages activated in the absence of glutamine compared to in complete medium, reflecting a marked and M2-specific downstream functional defect due to media perturbation (Figure 5E). The CCR2 transcript was expressed in only low amounts basally, and hence differential transcript expression did not translate to differences in surface protein expression (Figure S2D).

## TCA Breakpoint at IDH Coupled with Itaconate Synthesis Is a Major Feature of M1 Polarization

One of the major metabolic signatures of macrophage activation upon LPS stimulation is a defect in overall mitochondrial function (Biswas and Mantovani, 2012) and associated defects in the TCA cycle. However, the specific mechanism leading to such mitochondrial dysfunction is not understood. CoMBI-T analysis revealed a potential breakpoint in the metabolic flow of the TCA cycle at the isocitrate-to-oxoglutarate (AKG) conversion, which was specific to M1 versus M2 macrophages (Figure 3, green square). This effect was characterized by a significantly increased pool of (iso)citrate and decreased pool of AKG (the ratio of (iso)citrate:AKG is ~3 times higher in M1 compared to M0; Table S2) and was accompanied by significant transcriptional downregulation of *Idh1*, the enzyme that interconverts these two metabolites (7-fold decrease in M1). To further validate that this alteration of citrate and AKG steady-state levels results from reduced flow through IDH, we performed stable isotopic labeling experiments, tracing the fate of $^{13}$C-labels from U-$^{13}$C-glucose and U-$^{13}$C-glutamine in M1 macrophages with a single time point analysis to estimate relative rates of accumulation (4 hr labeling time). Consistent with CoMBI-T results, we observed that ~20% of citrate was synthesized from glucose, whereas the AKG pool accumulated 0% glucose-derived carbon labeling at the 4 hr time point (Figure 6). Carbon flow from glutamine to AKG was detectable in M1 macrophages (Figure 6: 10%–12% U-$^{13}$C-AKG from U-$^{13}$C-glutamine after 4 hr labeling), yet still significantly smaller than in the M0 state, where ~25% of the AKG pool acquired uniform labeling. Of note, partially labeled forms in the AKG pool present in M0 state reflective of active TCA cycling disappeared from the AKG pool in M1 macrophages (Figure 6, pie charts in black and green ovals next to AKG). Such a lack of partial labeling indicates interrupted TCA cycle activity and provides a mechanistic explanation for the

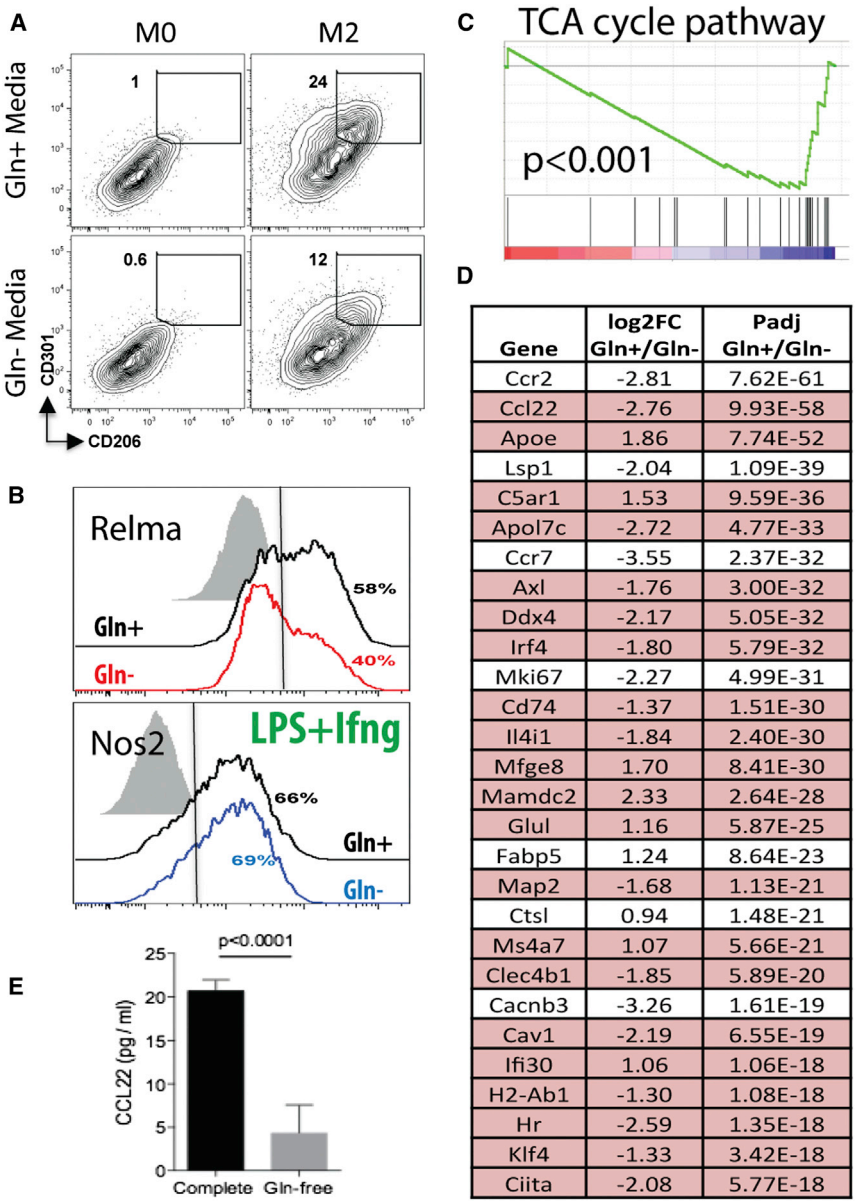


| Gene | log2FC Gln+/Gln- | Padj Gln+/Gln- |
|---|---|---|
| Ccr2 | -2.81 | 7.62E-61 |
| Ccl22 | -2.76 | 9.93E-58 |
| Apoe | 1.86 | 7.74E-52 |
| Lsp1 | -2.04 | 1.09E-39 |
| C5ar1 | 1.53 | 9.59E-36 |
| Apol7c | -2.72 | 4.77E-33 |
| Ccr7 | -3.55 | 2.37E-32 |
| Axl | -1.76 | 3.00E-32 |
| Ddx4 | -2.17 | 5.05E-32 |
| Irf4 | -1.80 | 5.79E-32 |
| Mki67 | -2.27 | 4.99E-31 |
| Cd74 | -1.37 | 1.51E-30 |
| Il4i1 | -1.84 | 2.40E-30 |
| Mfge8 | 1.70 | 8.41E-30 |
| Mamdc2 | 2.33 | 2.64E-28 |
| Glul | 1.16 | 5.87E-25 |
| Fabp5 | 1.24 | 8.64E-23 |
| Map2 | -1.68 | 1.13E-21 |
| Ctsl | 0.94 | 1.48E-21 |
| Ms4a7 | 1.07 | 5.66E-21 |
| Clec4b1 | -1.85 | 5.89E-20 |
| Cacnb3 | -3.26 | 1.61E-19 |
| Cav1 | -2.19 | 6.55E-19 |
| Ifi30 | 1.06 | 1.06E-18 |
| H2-Ab1 | -1.30 | 1.08E-18 |
| Hr | -2.59 | 1.35E-18 |
| Klf4 | -1.33 | 3.42E-18 |
| Ciita | -2.08 | 5.77E-18 |

**Figure 5. Labeling and Media Perturbation Experiments Validate the Critical Role of Glutamine in M2 Polarization**

(A) Glutamine deprivation shows significant (~50%) defect in M2 commitment in glutamine-deprived media based on CD301-CD206.

(B) Relmα staining and Nos2 upregulation indicate a comparative lack of effect for glutamine deprivation on M1 versus M2 commitment.

(C) Gene set enrichment analysis identifies significant transcriptional downregulation of TCA cycle.

(D) Top 30 differentially expressed genes between M2 macrophages polarized in full media versus glutamine-deprived media. Corresponding p values are shown for glutamine-no glutamine M2 macrophages, genes that are statistically different between M0 and M2 macrophages are indicated in red.

(E) Serum protein production of M2-specific chemokine CCL22 are downregulated when macrophages are polarized in glutamine-deprived conditions (error bars computed based on at least three independent experiments).

reports of mitochondrial dysfunction in M1 state. Notably, reverse flow at *Idh* is also undetectably low based on the absence of 5 carbon label from glutamine feed in citrate (from 5-labeled AKG).

It is important to point out that in the context of greatly reduced *Idh* activity and associated reduction of carbon flow to AKG, citric acid is redirected to serve as a precursor for itaconic acid synthesis, an important anti-microbial metabolite identified recently (Michelucci et al., 2013). Our U-$^{13}$C-glucose and U-$^{13}$C-glutamine labeling studies here are consistent with citrate serving as the direct chemical source for itaconic acid (Figure 6). Further supporting this possibility, we found *Irg1*, which encodes the enzyme catalyzing the aconitate-to-itaconate reaction (Michelucci et al., 2013), to be one of the most upregulated transcripts in M1 relative to M0 macrophages (Figure 3).

## Inflammatory Aspartate-Arginosuccinate Shunt Connects Anapleurosis of the TCA Cycle and NO Synthesis

The U-$^{13}$C-glutamine tracing experiments suggested an additional breakpoint in the TCA for M1 macrophages (Figure 7A). After 4 hr of labeling, initiated after 20 hr of exposure to LPS, approximately 35% of the succinate pool but only 22% of malate can be attributed to glutamine in M1s, as opposed to comparable labeling of these metabolites in M0 conditions (~39% and ~35%, respectively, Figure 7A). Additionally, the total pool of malate increased significantly in M1 conditions contrary to the only moderate increase in the steady-state concentration of succinate (see relative M0/M1 sizes of pie charts in Figure 7A). These data together suggest that the succinate-to-fumarate transition in M1 cells is not as efficient as it is in M0 macrophages, and there might be an alternative route for malate accumulation. Further examination revealed that the glutamine carbon-labeling pattern and M0/M1 pool ratio for malate were strikingly consistent to those observed for arginosuccinate, aspartate, and citrate (Figure 7A; Table S2). Such conserved labeling distribution patterns are characteristic of metabolites partaking in common metabolic cycles, in which pool sizes and labels are equilibrated among all members of the cycle, as illustrated by TCA cycle metabolites in M0 and M2 macrophages (Figure 4A). Notably, aspartate, arginosuccinate, malate, and fumarate are common components of the aspartate-arginosuccinate shunt (Lehninger et al., 2008), a set of transformations connecting the TCA cycle with the urea cycle (Allen et al., 2011), with active ornithine-to-citruline conversion. An inflammation-associated version of this shunt would account for the observed

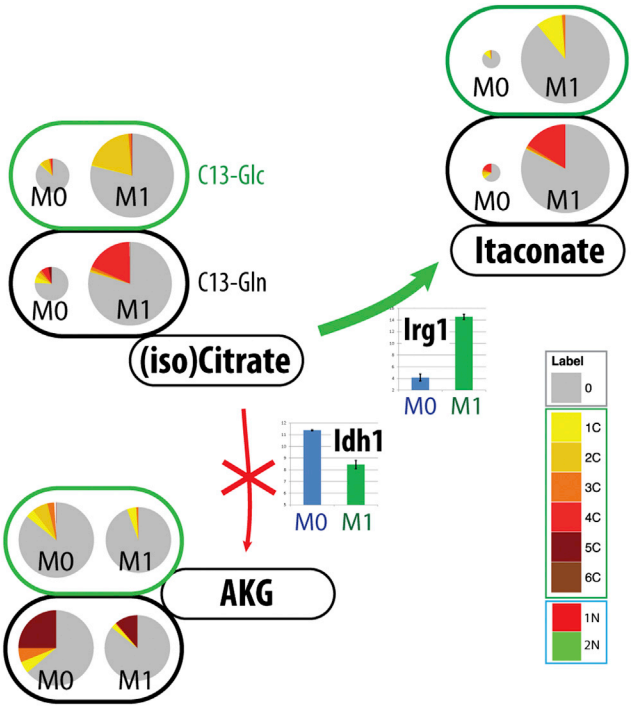


**Figure 6. A Breakpoint in TCA Cycle Is a Major Metabolic Marker of Macrophage M1 Polarization**

Labeling data show that (iso)citrate labeled by glucose does not transfer carbon to AKG in M1 macrophages, consistently with transcriptional downregulation of Idh1, resulting in isocitrate-to-2-oxoglutarate (AKG) transition blocked in M1-activated macrophages.

labeling patterns in these TCA intermediates and amino acids in M1 macrophages, connecting the TCA cycle metabolites with the NO cycle.

To functionally validate the importance of this apparent aspartate-arginosuccinate shunt, we pharmacologically inhibited the aspartate aminotransferase Got1 (marked with lightning in Figure 7A) by using aminooxyacetic acid (AOAA) (Kauppinen et al., 1987). As expected from the U-$^{13}$C-glutamine labeling results, pretreatment with AOAA at concentrations ranging from 1 to 10 μM inhibited M1 polarization as measured by NO production (Figure 7B) and by iNOS expression (Figure S3A, left) in a dose-dependent manner, although it did not affect macrophage viability (Figure S3B). Because NO production plays a role in the suppression of mitochondrial respiration in TLR-agonist-activated dendritic cells (Everts et al., 2012), we asked whether oxygen consumption rates (OCRs) increased in AOAA-treated M1 macrophages in which NO production was inhibited. As expected, untreated M1 macrophages exhibited very little mitochondrion-dependent (rotenone- and antimycin-inhibitable) oxygen consumption, and rather had very high, compensatory extracellular acidification rates (ECARs), a mark of exaggerated aerobic glycolysis (Everts et al., 2012). In contrast, M1 macrophages in which Got1/2 was inhibited retained mitochondrial respiratory function and exhibited ECARs similar to M0 macrophages (Figure 7C). This observation could reflect an inability of macrophages to execute anapleurosis of the TCA cycle in the presence of NO-based inhibition of succinate dehydrogenase if there is no proper balancing mechanism provided by the aspartate-aminotransferase as a part of aspartate-arginosuccinate shunt. Furthermore, we observe that perturbation of the shunt leads to profound functional consequences, such as a defect in inflammatory cytokine production, e.g., IL6 (Figure 7B, right).

## CoMBI-T Provides Insight into Redox Balance Regulation in M1-Polarized Macrophages

A related aspect of de novo fatty acid synthesis and the production of NO is the significant stoichiometric demand for nicotinamide adenine dinucleotide phosphate (NADPH) in these processes (Knowles and Moncada, 1994). Another NADPH-demanding process is the regulation of reactive oxygen species (ROS) levels, mediated in M1 macrophages by *Cybb*-encoded NADPH oxidase (Nox2), which we found to be transcriptionally upregulated in M1 macrophages and downregulated in M2 cells (Figure S4). Downregulation of *Idh* in M1-polarized cells compromises one of the sources for NADPH (Geisbrecht and Gould, 1999). In the context of macrophage polarization, two major sources of NADPH production are typically discussed: conversion of malate to pyruvate by malic enzyme and the oxidative branch of the pentose phosphate pathway (PPP), which was previously shown to play a role in macrophage polarization (Haschemi et al., 2012) and is also one of the seven M1 versus M2 defining modules identified by CoMBI-T (Figure 3). In our data, we did not detect signatures of malic enzyme activity in M1 macrophages, corresponding to labeled pyruvate or lactate from U-$^{13}$C-glutamine (Figures S5A and S5B). We did, however, confirm significant carbon flow through the oxidative arm of PPP (Haschemi et al., 2012) in M1 macrophages by using $^{13}$C-glucose carbon tracing experiments, finding that both the total pool of pentose-5-phosphates and their labeled fraction increased significantly in M1 relative to M0 cells (Figure S5C). In addition to the previously described role of Carkl (Haschemi et al., 2012), metabolic and transcriptional regulation of the PPP pathway was indicated by the relation of levels of early PPP metabolites (D-Glucono-1,5-lactone 6-phosphate and 6-Phospho-D-gluconate, Figure 3) and transcriptional regulation of the downstream enzyme Pgd that converts 6-Phospho-D-gluconate to ribulose-5P. Pgd's upregulation under M1 conditions (Figure S6A) is consistent with increased flux through the PPP, leading to a decrease in steady-state levels of early PPP metabolites relative to levels in M0 and M2 cells (hence, these metabolites are marked in red in Figure 3). These effects of oxidative stress are typically counterbalanced by reducing agents such as glutathione, and indeed, we observed coordinated transcriptional regulation of glutathione reductase (Gsr, upregulated in M1 cells) and glutathione peroxidase (Gpx1, downregulated in M1 cells) (Figure S6B), which was consistent with labeling data showing increased labeling of oxidized glutathione by glutamine-derived carbon in M1, but not M2, macrophages (Figure S6C).

## DISCUSSION

In this work, we developed a pipeline for high-throughput parallel metabolic and transcriptional data profiling with integration of these datasets that allows non-targeted identification of

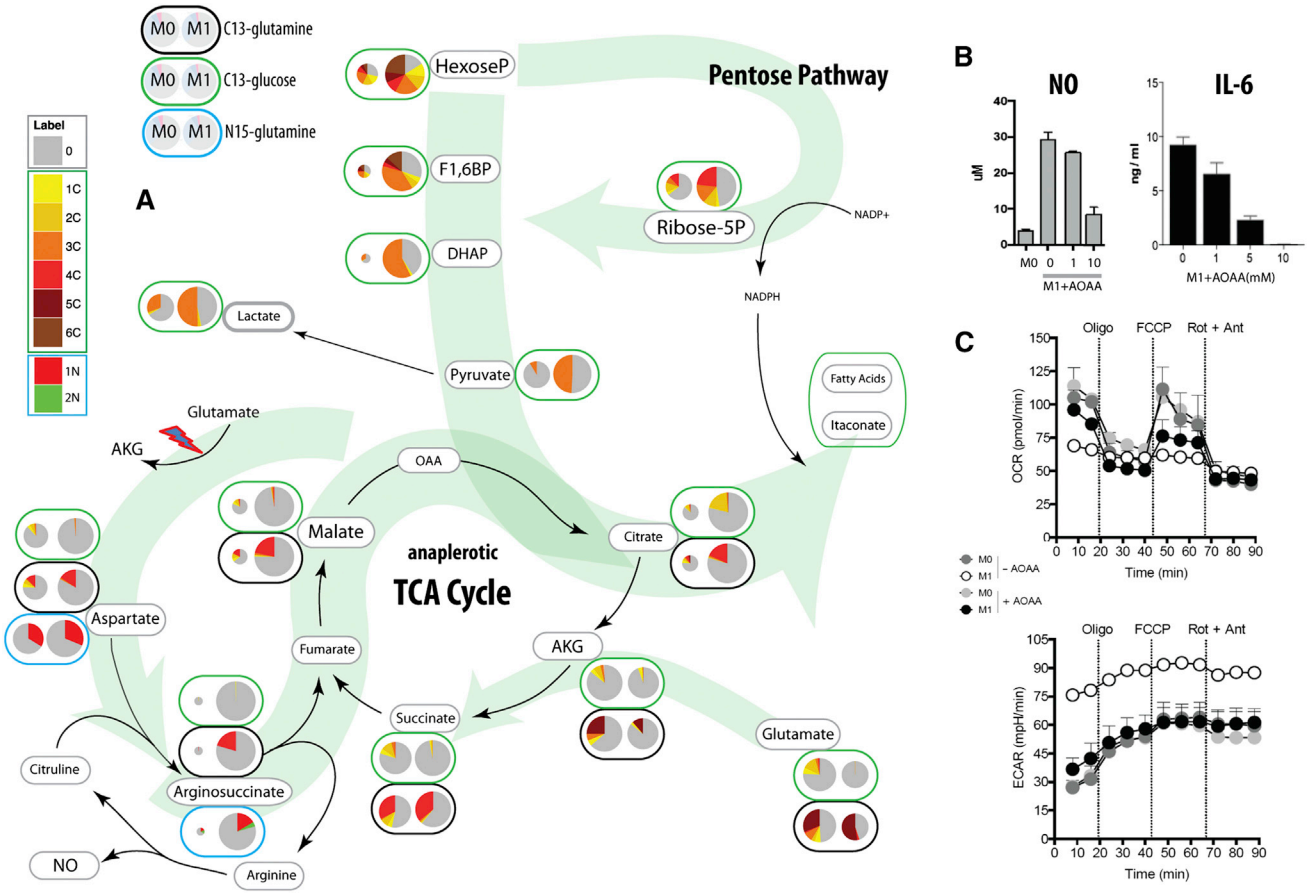


**Figure 7. Labeling Data Reveal an Inflammatory Version of the Aspartate-Arginoscucinate Shunt in M1-Polarized Macrophages**

(A) U-$^{13}$C glucose (green outline), U-$^{13}$C (black outline), and $^{15}N_2$-glutamine (blue outline) were used as media for unstimulated and M1-stimulated macrophages. Circle sizes are scaled with respect to pool sizes for individual metabolites in each condition. Exact labeling distributions and patterns are detailed in Table S2 for each metabolite.

(B) Inhibition of Got1/2 (aspartate-aminotransferase, marked with lightning sign in A) with AOAA decreases nitric oxide and IL-6 production in a dose-dependent manner without affecting macrophage viability (Figure S3B) (error bars computed based on at least three independent experiments).

(C) SeaHorse data on oxygen consumption rate (OCR) and extracellular acidification rates (ECAR), both rotenone and antimycin inhibited, and very high, compensatory M1 macrophages in which Got1/2 was inhibited, retain mitochondrial respiratory function (top), and exhibited ECARs similar to M0 macrophages (bottom).

regulated metabolic modules. We applied this approach to uncover an integrated global picture of the metabolic rewiring that characterizes macrophage polarization and revealed a set of known and novel modules that define the M1- and M2-polarized states, including the UDP-GlcNAc biosynthesis pathway, glutamine-related pathway flows, an M1-specific TCA cycle breakpoint at *Idh*, and the engagement of aspartate-arginosuccinate shunt to balance carbon flow in the presence of NO production. We additionally confirmed previously recognized metabolic features, such as elevated glycolytic activity and reduction in oxidative phosphorylation activity upon polarization to M1, which are metabolically consistent with, and gain mechanistic context from, our findings of flux discontinuity within the canonical TCA cycle (at Idh and succinate dehydrogenase). The discontinuity at Idh is evident at both the transcriptional and the steady-state metabolic level and was confirmed by the pathway flow studies. The metabolic role of this pathway flow constriction downstream of isocitrate, in parallel with high carbon flow into the TCA upstream of citrate, appears to be the metabolic mechanism to enable significant production of large pools of fatty acids and itaconate, which exhibits a labeling pattern identical with its upstream precursors citrate/isocitrate (the LCMS methods used here do not distinguish the two citrate isomers). Itaconate itself was recently described as an important anti-microbial agent, disrupting the glyoxylate shunt, a pathway used in some pathogens (e.g., *Mycobacterium tuberculosis*) but not mammalian cells (Michelucci et al., 2013). The significance of flux re-direction in M1 macrophages at the level of citrate/aconitate is also evident from recent studies, where knock-down of the mitochondrial citrate carrier was shown to lead to defects in macrophage activation in response to LPS (Infantino et al., 2011; O'Neill, 2011) due to blocking production of cytosolic AcCoA. Overall, our data show that the module embodying citrate/isocitrate, *Irg1*, and itaconate constitutes a systems-level marker of M1 polarization that is at least as robust as the well-established *Cox2*-PGE2 and *iNOS*-NO transcriptional-metabolic duos (see Figure 3).

Analysis of labeling patterns in M1 macrophages supports a role for the aspartate-arginosuccinate shunt in coordinating the NO cycle with anapleurosis of the TCA cycle. Such a route of anapleurosis would likely be necessary in the context of a TCA breakpoint at succinate dehydrogenase. Note that the flow from aspartate to oxaloacetate via aspartate transaminase replenishes the cycle immediately downstream of this break and provides substrate for citrate synthase to handle an increased flux producing itaconic acid from the same carbon skeleton. Functionally, inhibition of aspartate transaminase led to a decrease in NO production and the maintenance of mitochondrial respiration, a finding that is consistent with the known inhibitory effects of NO on the electron transport chain (Everts et al., 2012). The ability of AOAA to inhibit NO production has been previously demonstrated for astrocytes (Schmidlin and Wiesinger, 1998), where the transamination inhibitor eliminates flow from the aspartate nitrogen to citruline and the citruline-arginine-NO cycle. These findings indicate that the aspartate-arginosuccinate shunt might be an adaptation to the fact that NO, a major effector molecule of M1 macrophages, competes with oxygen to inhibit complex II of the electron transport chain and, by doing so, attenuates succinate-to-fumarate conversion creating the aforementioned second break-point in the TCA cycle (Stadler et al., 1991). Furthermore, the presence of this break point would be consistent with the release of succinate from the local metabolic network, enabling it to participate in signaling pathways that are central to M1 polarization such as IL-1β induction (Tannahill et al., 2013).

CoMBI-T analysis allowed us to identify two pathways critical for M2 polarization: glutamine-related metabolism and the UDP-GlcNAc pathway. These features of M2 polarization have, to the best of our knowledge, not been discussed previously. We found that transient glutamine deprivation had negative effects on the M2 activation program, which was associated with its effects on the TCA cycle. mTOR signaling has been shown to regulate macrophage polarization (Byles et al., 2013) and prolonged or harsher starvation conditions will probably lead to an interesting interplay between macrophage polarization, metabolism, and mTOR signaling, which is an exciting avenue for future exploration. Moreover, targeted inhibition of N-glycosylation, a pathway highlighted in M2 macrophages and one that requires UDP-GlcNAc as a sugar donor, also inhibited M2 activation (as measured by Relmα, CD206, and CD301 expression). This finding, which could reflect the requirement for N-glycosylation to correctly fold and traffic proteins such as Relmα, CD206, and CD301, which are destined for export to the cell surface, or for secretion, emphasizes the importance of glutamine-dependent pathways in these cells. Our findings do not exclude the possibility that UDP-GlcNAc is also serving as a sugar donor for O-glycosylation, a pathway that is recognized to serve as a major connecting hub between cellular metabolism and signaling (Wellen and Thompson, 2012). The dependence of M2 activation on glutamine is intriguing not least because of the recognized role of M2 macrophages in wound healing (Murray and Wynn, 2011) and the findings that glutamine supplementation might provide a viable means to support recovery after surgery (Wilmore, 2001).

We are optimistic that these findings summarized above will spur activity into the development of approaches to manipulate the newly identified metabolic modules to affect macrophage function in clinically relevant settings.

## EXPERIMENTAL PROCEDURES

### Animals and Mouse Bone-Marrow-Derived Macrophage Culture

C57BL/6J (The Jackson Laboratory) mice were bred and maintained under specific-pathogen-free conditions according to protocols approved by the institutional animal care at Washington University School of Medicine and were used at age of 8–12 weeks. BM cells were harvested from femurs and tibia of C57BL6/J mice and differentiated in the presence of recombinant mouse M-CSF (20 ng/ml; R&D Systems) in complete RPMI 1640 (Corning) containing 10 mM glucose, 2 mM L-glutamine, 100 U/ml of penicillin/streptomycin, and 10% FCS for 7 days. Day 7 BMDMs were washed and cultured in presence or absence (for 4 hr) of 2 mM glutamine medium containing 10 mM glucose and 10% dialyzed FCS prior to IL-4 (20 ng/ml; PeproTech) or lipopolysaccharide (LPS, 20 ng/ml; Sigma) + IFN-γ (50 ng/ml; R&D Systems) 24 hr stimulation. In Got1/2 inhibition experiments, day 7 BMDMs were treated for 1 hr with 10 mM, 5 mM, or 1 mM aminooxacetic acid (AOAA; Sigma) prior to 24 hr stimulation with LPS + IFN-γ. For inhibition of N-glycosylation, tunicamycin (1 μM or 2 μM as indicated; Sigma) was added on day 7 BMDMs 1 hr prior to 24 hr stimulation with IL-4.

### Quantification of CCL22, IL-6, and Nitric Oxide in Culture Supernatants

CCL22, IL-6, and nitric oxide concentrations were determined with, respectively, the CCL22/MDC DuoSet ELISA kit (R&D Systems), the IL-6 ELISA Ready-Set-Go! Kit, and the Griess Reagent System (Promega), according to manufacturers' instructions.

### Flow Cytometry and Extracellular Flux Analysis

Cells were blocked with 5 μg/ml of anti-CD16/32 (clone 93, eBiosciences) before the surface staining with antibodies to F4/80 (clone BM8, eBiosciences), CD206 (clone C068C2, Biolegend), CD301 (clone ER-MP23, AbD Serotec). For intracellular staining of RELMα and iNOS, cells were fixed with a fixation buffer (BD Biosciences) and stained with rabbit anti-RELMα (PeproTech) and mouse anti-NOS2 (clone C-11; Santa Cruz Biotechnology), followed by incubation with appropriate fluorochrome-conjugated anti-rabbit or anti-mouse IgG (both Jackson Immunoresearch). Cells were also stained with LIVE/DEAD (Invitrogen) or 7-amino-actinomycin D (eBiosciences). Data were acquired on a FACSCanto II flow cytometer (BD Biosciences) and analyzed with FlowJo v.9.5.2 (Tree Star). Measurements of oxygen consumption rates and extracellular acidification rates were made with a Seahorse extracellular flux analyzer as described previously (Everts et al., 2012, 2014).

### LC-MS and Data Analysis for Metabolomics

Data generated from a Quadrupole Time-of-flight mass spectrometer was used as the MS input for our CoMBI-T analysis; all steps of MS data processing were performed with Matlab R2010b (The Mathworks) using functions native to the Bioinformatics, Statistics, Database, and Parallel Computing toolboxes (Fuhrer et al., 2011). For the subsequent isotopic labeling experiments to validate the CoMBI-T findings (amino acid and central metabolite analyses), either triple-quadrupole MS data were acquired using scheduled selective reaction monitoring (SRM) in negative mode, or high-resolution accurate mass (HRAM) LC-MS data were acquired with a QExactive Orbitrap mass spectrometer (Thermo Fisher Scientific), in either positive or negative mode as appropriate; acquisition was controlled by Xcalibur 2.2 software (Thermo Fisher Scientific). U-$^{13}$C-L-glutamine and U-$^{13}$C-D-glucose were purchased from Sigma. Cell extracts were prepared from live cultures on Hamilton StarPlus system running an automated metabolite extraction protocol using hot 70% aq. ethanol (70°C). Supernatant of extracted samples were dried under vacuum and resuspended in LC-MS grade water for analysis of the relative abundance of $^{13}$C and $^{15}$N metabolites (Munger et al., 2008).

### RNA Sequencing

mRNA was extracted from cell lysates by means of oligo-dT beads (Invitrogen). For cDNA synthesis, we used custom oligo-dT primer with a barcode and adaptor-linker sequence (CCTACACGACGCTCTTCCGATCT-XXXX XXXX-T15). After first-strand synthesis, samples were pooled together based on Actb qPCR values and RNA-DNA hybrid was degraded with consecutive acid-alkali treatment. Then, a second sequencing linker (AGATCGGAAGAG

CACACGTCTG) was ligated with T4 ligase (NEB) followed by SPRI clean-up. The mixture then was PCR enriched 12 cycles and SPRI purified to yield final strand-specific RNA-seq libraries. Data were sequenced on HiSeq 2500 by'/ 50bpX25bp pair-end sequencing. Second mate was used for sample demultiplexing, at which point individual single-end fastqs were aligned to mm9 genome via TopHat and gene expression was obtained via ht-seq and DESeq2 for differential expression.

### Integrated Network Analysis

To construct the network for integrated analysis of metabolomic and RNA-seq data, we downloaded KEGG REACTION, KEGG ENZYME, KEGG COMPOUND, and KEGG GLYCAN databases (August 2013 version) (Kanehisa et al., 2012). Additionally, the reaction converting *cis*-aconitate to itaconate controlled by *Irg1* (Michelucci et al., 2013) was added to the network manually. A global combined network that connects nodes representing reactions to the nodes representing metabolites was constructed, in which nodes representing each reaction are connected to its respective substrates and products. Then we mapped reactions to enzymes REACTION and ENZYME databases. COMPOUND and GLYCAN databases were used to algorithmically access names for compounds. Reactions lacking at least one enzyme with an associated mouse gene were excluded from the network; sub-reactions embedded in multi-step metabolic transformations were masked, keeping only net reaction in the network. Based on names, anomeric metabolites were collapsed into a single species. Then we masked some common highly connected metabolites in the network: non-organic metabolites (water, ammonia, etc.), (deoxy)nucleosides phosphates (ATP, ADP, dATP, etc.), common cofactors (NADH, FAD, etc.), some generic metabolites (acceptors, ROH, etc.), and ubiquitin. The resulting network represents topological description of murine metabolism, independent of specific data. After data acquisition and application to the integrated model network, p values for metabolites and genes were calculated with limma and DESeq R-packages for differential expressions (Anders and Huber, 2010). For analysis, reactions with transcripts not detected in any sample (number of matching reads <5, leading to 14,276 significantly expressed genes) were excluded from the network. Next, reactions were assigned a differential regulation p value, corresponding to a differential expression p value for the transcript specific to the reaction. In cases where more than one enzyme (transcript) was associated with the reaction, we selected the single enzyme (transcript) that had the minimal p value; these p values were assigned as reaction p values. Then groups of reactions having at least one common metabolite and a shared most-significant gene were collapsed into single nodes. The problem for finding most significant module in the network was thus reduced to a maximum-weight connected subgraph (MWCS) problem (Beisser et al., 2010). Scores were assigned to all metabolites and reactions based on their p values and FDR threshold fitting a FitBumModel distribution separately to metabolites and genes: metabolite and reaction p values with low p value had positive scores; ones with high p values had negative scores. The score for metabolites absent from the data is a parameter and was chosen to be $-10$. MWCS instances were solved by heinz solver (http://www.mi.fu-berlin.de/w/LiSA/Heinz). Resulting networks were annotated and plotted in Cytoscape.

## ACCESSION NUMBERS

Raw and processed sequencing data are deposited to PubMed GEO under GSE53053.

## SUPPLEMENTAL INFORMATION

Supplemental Information includes six figures, two tables, and Supplemental Experimental Procedures and can be found with this article online at http://dx.doi.org/10.1016/j.immuni.2015.02.005.

## ACKNOWLEDGMENTS

We would like to thank Eugene Oltz for useful comments and help with the manuscript. We would also like to thank Ananya Mukherjee for helping with the figures used in the manuscript. M.N.A. would like to thank J.A. for support and stimulating discussions. E.M.D. declares competing financial interest as a founder and shareholder of General Metabolics. K.C., K.M.S., and A.K.J. were employees of Agios when this study was conducted.

Received: April 29, 2014
Revised: November 24, 2014
Accepted: January 15, 2015
Published: March 17, 2015

## REFERENCES

Allen, A.E., Dupont, C.L., Oborník, M., Horák, A., Nunes-Nesi, A., McCrow, J.P., Zheng, H., Johnson, D.A., Hu, H., Fernie, A.R., and Bowler, C. (2011). Evolution and metabolic significance of the urea cycle in photosynthetic diatoms. Nature *473*, 203–207.

Anders, S., and Huber, W. (2010). Differential expression analysis for sequence count data. Genome Biol. *11*, R106.

Beisser, D., Klau, G.W., Dandekar, T., Müller, T., and Dittrich, M.T. (2010). BioNet: an R-Package for the functional analysis of biological networks. Bioinformatics *26*, 1129–1130.

Beisser, D., Grohme, M.A., Kopka, J., Frohme, M., Schill, R.O., Hengherr, S., Dandekar, T., Klau, G.W., Dittrich, M., and Müller, T. (2012). Integrated pathway modules using time-course metabolic profiles and EST data from *Milnesium tardigradum*. BMC Syst. Biol. *6*, 72.

Biswas, S.K., and Mantovani, A. (2012). Orchestration of metabolism by macrophages. Cell Metab. *15*, 432–437.

Bordbar, A., Mo, M.L., Nakayasu, E.S., Schrimpe-Rutledge, A.C., Kim, Y.M., Metz, T.O., Jones, M.B., Frank, B.C., Smith, R.D., Peterson, S.N., et al. (2012). Model-driven multi-omic data analysis elucidates metabolic immunomodulators of macrophage activation. Mol. Syst. Biol. *8*, 558.

Byles, V., Covarrubias, A.J., Ben-Sahra, I., Lamming, D.W., Sabatini, D.M., Manning, B.D., and Horng, T. (2013). The TSC-mTOR pathway regulates macrophage polarization. Nat. Commun. *4*, 2834.

Everts, B., Amiel, E., van der Windt, G.J., Freitas, T.C., Chott, R., Yarasheski, K.E., Pearce, E.L., and Pearce, E.J. (2012). Commitment to glycolysis sustains survival of NO-producing inflammatory dendritic cells. Blood *120*, 1422–1431.

Everts, B., Amiel, E., Huang, S.C., Smith, A.M., Chang, C.H., Lam, W.Y., Redmann, V., Freitas, T.C., Blagih, J., van der Windt, G.J., et al. (2014). TLR-driven early glycolytic reprogramming via the kinases TBK1-IKKε supports the anabolic demands of dendritic cell activation. Nat. Immunol. *15*, 323–332.

Fuhrer, T., Heer, D., Begemann, B., and Zamboni, N. (2011). High-throughput, accurate mass metabolome profiling of cellular extracts by flow injection-time-of-flight mass spectrometry. Anal. Chem. *83*, 7074–7080.

Geisbrecht, B.V., and Gould, S.J. (1999). The human PICD gene encodes a cytoplasmic and peroxisomal NADP(+)-dependent isocitrate dehydrogenase. J. Biol. Chem. *274*, 30527–30533.

Haschemi, A., Kosma, P., Gille, L., Evans, C.R., Burant, C.F., Starkl, P., Knapp, B., Haas, R., Schmid, J.A., Jandl, C., et al. (2012). The sedoheptulose kinase CARKL directs macrophage polarization through control of glucose metabolism. Cell Metab. *15*, 813–826.

Infantino, V., Convertini, P., Cucci, L., Panaro, M.A., Di Noia, M.A., Calvello, R., Palmieri, F., and Iacobazzi, V. (2011). The mitochondrial citrate carrier: a new player in inflammation. Biochem. J. *438*, 433–436.

Kanehisa, M., Goto, S., Sato, Y., Furumichi, M., and Tanabe, M. (2012). KEGG for integration and interpretation of large-scale molecular data sets. Nucleic Acids Res. *40*, D109–D114.

Kauppinen, R.A., Sihra, T.S., and Nicholls, D.G. (1987). Aminooxyacetic acid inhibits the malate-aspartate shuttle in isolated nerve terminals and prevents the mitochondria from utilizing glycolytic substrates. Biochim. Biophys. Acta *930*, 173–178.

Knowles, R.G., and Moncada, S. (1994). Nitric oxide synthases in mammals. Biochem. J. *298*, 249–258.

Koch, H.U., Schwarz, R.T., and Scholtissek, C. (1979). Glucosamine itself mediates reversible inhibition of protein glycosylation. A study of glucosamine metabolism at inhibitory concentrations in influenza-virus-infected cells. Eur. J. Biochem. *94*, 515–522.

Lehninger, A., Nelson, D., and Cox, M. (2008). Lehninger Principles of Biochemistry. (W.H. Freeman), p. 684.

McGettrick, A.F., and O'Neill, L.A. (2013). How metabolism generates signals during innate immunity and inflammation. J. Biol. Chem. *288*, 22893–22898.

Michelucci, A., Cordes, T., Ghelfi, J., Pailot, A., Reiling, N., Goldmann, O., Binz, T., Wegner, A., Tallam, A., Rausell, A., et al. (2013). Immune-responsive gene 1 protein links metabolism to immunity by catalyzing itaconic acid production. Proc. Natl. Acad. Sci. USA *110*, 7820–7825.

Munger, J., Bennett, B.D., Parikh, A., Feng, X.J., McArdle, J., Rabitz, H.A., Shenk, T., and Rabinowitz, J.D. (2008). Systems-level metabolic flux profiling identifies fatty acid synthesis as a target for antiviral therapy. Nat. Biotechnol. *26*, 1179–1186.

Murray, P.J., and Wynn, T.A. (2011). Protective and pathogenic functions of macrophage subsets. Nat. Rev. Immunol. *11*, 723–737.

O'Neill, L.A. (2011). A critical role for citrate metabolism in LPS signalling. Biochem. J. *438*, e5–e6.

O'Neill, L.A., and Hardie, D.G. (2013). Metabolism of inflammation limited by AMPK and pseudo-starvation. Nature *493*, 346–355.

Patil, K.R., and Nielsen, J. (2005). Uncovering transcriptional regulation of metabolism by using metabolic network topology. Proc. Natl. Acad. Sci. USA *102*, 2685–2689.

Rodríguez-Prados, J.C., Través, P.G., Cuenca, J., Rico, D., Aragonés, J., Martín-Sanz, P., Cascante, M., and Boscá, L. (2010). Substrate fate in activated macrophages: a comparison between innate, classic, and alternative activation. J. Immunol. *185*, 605–614.

Schmidlin, A., and Wiesinger, H. (1998). Argininosuccinate synthetase: localization in astrocytes and role in the production of glial nitric oxide. Glia *24*, 428–436.

Shanware, N.P., Bray, K., Eng, C.H., Wang, F., Follettie, M., Myers, J., Fantin, V.R., and Abraham, R.T. (2014). Glutamine deprivation stimulates mTOR-JNK-dependent chemokine secretion. Nat. Commun. *5*, 4900.

Sica, A., and Mantovani, A. (2012). Macrophage plasticity and polarization: in vivo veritas. J. Clin. Invest. *122*, 787–795.

Sojka, D.K., Plougastel-Douglas, B., Yang, L., Pak-Wittel, M.A., Artyomov, M.N., Ivanova, Y., Zhong, C., Chase, J.M., Rothman, P.B., Yu, J., et al. (2014). Tissue-resident natural killer (NK) cells are cell lineages distinct from thymic and conventional splenic NK cells. eLife *3*, e01659.

Stadler, J., Billiar, T.R., Curran, R.D., Stuehr, D.J., Ochoa, J.B., and Simmons, R.L. (1991). Effect of exogenous and endogenous nitric oxide on mitochondrial respiration of rat hepatocytes. Am. J. Physiol. *260*, C910–C916.

Tannahill, G.M., Curtis, A.M., Adamik, J., Palsson-McDermott, E.M., McGettrick, A.F., Goel, G., Frezza, C., Bernard, N.J., Kelly, B., Foley, N.H., et al. (2013). Succinate is an inflammatory signal that induces IL-1$\beta$ through HIF-1$\alpha$. Nature *496*, 238–242.

Varki, A. (2009). Essentials of Glycobiology, Second Edition. (Cold Spring Harbor Laboratory Press).

Vats, D., Mukundan, L., Odegaard, J.I., Zhang, L., Smith, K.L., Morel, C.R., Wagner, R.A., Greaves, D.R., Murray, P.J., and Chawla, A. (2006). Oxidative metabolism and PGC-1beta attenuate macrophage-mediated inflammation. Cell Metab. *4*, 13–24.

Wellen, K.E., and Thompson, C.B. (2012). A two-way street: reciprocal regulation of metabolism and signalling. Nat. Rev. Mol. Cell Biol. *13*, 270–276.

Wilmore, D.W. (2001). The effect of glutamine supplementation in patients following elective surgery and accidental injury. J. Nutr. *131*, 2543S–2549S, discussion 2550S–2551S.

Yi, W., Clark, P.M., Mason, D.E., Keenan, M.C., Hill, C., Goddard, W.A., 3rd, Peters, E.C., Driggers, E.M., and Hsieh-Wilson, L.C. (2012). Phosphofructokinase 1 glycosylation regulates cell growth and metabolism. Science *337*, 975–980.

Zhu, J., Sova, P., Xu, Q., Dombek, K.M., Xu, E.Y., Vu, H., Tu, Z., Brem, R.B., Bumgarner, R.E., and Schadt, E.E. (2012). Stitching together multiple data dimensions reveals interacting metabolomic and transcriptomic networks that modulate cell regulation. PLoS Biol. *10*, e1001301.